

pubs.acs.org/IECR Article

Phase Equilibria, Diffusivities, and Equation of State Modeling of HFC-32 and HFC-125 in Imidazolium-Based Ionic Liquids for the Separation of R-410A

Ana Rita C. Morais, Abby N. Harders, Kalin R. Baca, Greta M. Olsen, Bridgette J. Befort, Alexander W. Dowling, Edward J. Maginn, and Mark B. Shiflett*



Cite This: Ind. Eng. Chem. Res. 2020, 59, 18222-18235



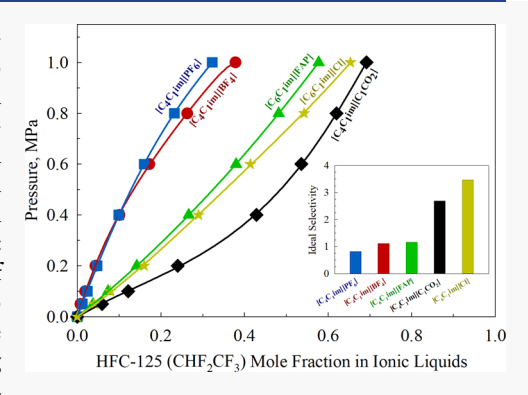
ACCESS

Metrics & More

Article Recommendations

Supporting Information

ABSTRACT: Growing concerns about the global warming potential of hydro-fluorocarbons (HFCs) has led to increasing interest in developing technologies to effectively recover and recycle these refrigerants. Ionic liquids (ILs) have shown great potential to selectively separate azeotropic HFC gas mixtures, such as R-410A composed of HFC-32 (CH₂F₂) and HFC-125 (CHF₂CF₃), based on solubility differences between the refrigerant gases in the respective IL. Isothermal vapor—liquid equilibrium (VLE) data for HFC-32 and HFC-125 were measured in ILs containing fluorinated and nonfluorinated anions using a gravimetric microbalance at pressures ranging from 0.05 to 1.0 MPa and a temperature of 298.15 K. The van der Waals equation of state (EoS) model was applied to correlate the experimental solubility data of each HFC refrigerant/IL mixture. The solubility differences between HFC-32 and HFC-125 vary significantly depending on the choice of IL. The diffusion coefficients for both HFC refrigerants in each IL



were calculated by fitting Fick's law to time-dependent absorption data. HFC-32 has a higher diffusivity in most ILs tested because of its smaller molecular radius relative to HFC-125. Based on the calculated Henry's law constants and the mass uptake for each system, $[C_6C_1\text{im}][Cl]$ was found to have the highest selectivity difference for separating R-410A at 298.15 K.

1. INTRODUCTION

Hydrofluorocarbons (HFCs) are a family of refrigerants extensively used in air-conditioning and refrigeration systems. HFCs were developed to replace chlorofluorocarbons that were linked to the depletion of the earth's ozone layer. HFCs have zero ozone depletion potential (ODP),¹ but some have high global warming potential (GWP).^{2,3} The Kyoto Protocol of the United Nations Framework Convention on Climate Change (UNFCCC)⁴ has recommended the phase-out of HFCs under the Kigali Amendment to the Montreal Protocol.⁵ In addition, the EU Regulation no. 517/2014 that mandates the reduction of up to two-thirds of the 2010 fluorinated greenhouse gas emissions by 2030 has been implemented.⁶

R-410A is a near-azeotropic HFC mixture composed of 50.0 mass % HFC-32 (CH₂F₂, NBPT = 221.3 K) (normal boiling point temperature) and 50.0 mass % HFC-125 (CHF₂CF₃, NBPT = 224.9 K) that was developed as a replacement for HCFC-22 (CHClF₂) in residential and commercial airconditioning and heat pump systems.⁷ Currently, there is no commercial technology available for separation of HFC-32 and HFC-125; therefore, if R-410A cannot be recycled in the future, it will have to be incinerated.^{8,9} The need for a sustainable process to separate R-410A such that HFC-32 can be used in low-GWP blends with hydrofluoroolefins (HFOs), and HFC-125 can be utilized as a feedstock for future products

is critically important considering the pending and new regulations that will limit the use of HFCs.

Ionic liquids (ILs) are of particular interest for absorption-based gas separation processes. These low-melting salts, which are composed of an organic cation, such as imidazolium, pyridinium, and ammonium, combined with either an organic (e.g., HCOO⁻ and CH₃COO⁻) or an inorganic anion (e.g., Cl⁻, BF₄⁻, and PF₆⁻), can be molecularly designed to selectively increase the solubility of either HFC-32 or HFC-125 for the optimal separation of R-410A. Many ILs have a negligible vapor pressure, which makes them ideal entrainers for gas separation processes because of the minimal loss to the gas phase. ILs provide opportunities to develop new gas separation technologies because of their high chemical and thermal stability with HFCs. While a large number of publications available in the literature focus on the use of ILs for separation and purification of natural gases, such as CO₂/

Received: June 5, 2020
Revised: September 3, 2020
Accepted: September 4, 2020
Published: September 4, 2020





$$F = \begin{matrix} F \\ F \\ F \end{matrix}$$

$$F = \begin{matrix} F \\ F \\ F \end{matrix}$$

$$Diffluoromethane Pentafluoroethane (HFC-32) (HFC-125)$$

$$1-butyl-3-methylimidazolium acetate ([C_4C_1im][C_1CO_2]) ([C_4C_1im][BF_4])$$

$$1-butyl-3-methylimidazolium hexafluorophosphate ([C_4C_1im][PF_6]) ([C_6C_1im][FAP])$$

$$1-butyl-3-methylimidazolium thiocyanate ([C_6C_1im][FAP])$$

$$1-butyl-3-methylimidazolium thiocyanate ([C_6C_1im][C1]) ([C_6C_1im][C1])$$

Figure 1. Chemical structures and acronyms of the HFC refrigerants and ILs.

CH₄¹¹ and CO₂/N₂,¹² not many reports have been published on the use of ILs for the separation of azeotropic HFC refrigerant mixtures. Shiflett and Yokozeki proposed using ILs to separate R-507 [50 wt % HFC-125 and 50 wt % HFC-143a (1,1,1-trifluoroethane, CH₃CF₃)] and R-404a [44 wt % HFC-125, 52 wt % HFC-143a and 4 wt % HFC-134a (1,1,1,2tetrafluoroethane, CH₂FCF₃)] when they discovered large differences in the solubility of HFCs in 1-butyl-3-methylimidazolium tetrafluoroborate $[C_4C_1\text{im}][BF_4]$ and 1-butyl-3methylimidazolium hexafluorophosphate $[C_4C_1im][PF_6]^{.13}$ Also, the same authors investigated the use of $[C_4C_1im][PF_6]$ as an entraining agent for extractive distillation to separate R-410A into HFC-32 and HFC-125.14 The separation was simulated using ASPEN Plus and resulted in an efficient separation of R-410A into 99 mol % HFC-32 and 99 mol % HFC-125. Additional measurements on HFC-32 and HFC-125 in ILs have been recently conducted by Sosa et al., Liu et al., Sousa et al., and Asensio-Delgado et al. 15-20

The present study aims to contribute to the development and implementation of IL-based separation processes for recovering and recycling of HFC refrigerants. To assess the impact of varying the anions has on solubility and diffusivity, imidazolium-based cations with a range of different anions were examined. This was done to test the hypothesis that anions have a larger effect on physical gas solubility than cations. In this context, the vapor—liquid equilibria (single-component absorption) of the R-410A components, that is, HFC-32 and HFC-125, in 1-butyl-3-methylimidazolium acetate ($[C_4C_1im][C_1CO_2]$), $[C_4C_1im][BF_4]$, $[C_4C_1im][PF_6]$, 1-butyl-3-methylimidazolium thiocyanate ($[C_4C_1im][SCN]$),

1-hexyl-3-methylimidazolium chloride ($[C_6C_1\text{im}][Cl]$), and 1-hexyl-3-methylimidazolium tris(pentafluoroethyl)-trifluorophosphate ($[C_6C_1\text{im}][FAP]$) were measured using a gravimetric microbalance at 298.15 K and pressures up to 1.0 MPa. The temperature of 298.15 K was chosen for this study to screen ILs for capacity and selectivity differences. The most promising candidates will be studied in more depth over a range of temperatures in the future.

One of the motivations for this work is to develop a framework where accurate engineering models can be developed and used for process optimization to select the best IL from a total cost and performance standpoint. No single IL property, such as solubility or viscosity, can be used to make such an assessment. The van der Waals (EoS) model was applied to correlate and predict the phase equilibria for each HFC-32/IL and HFC-125/IL mixture using the experimental solubility data. In addition, the time-dependent behavior of the HFC/IL systems was analyzed using the one-dimensional Fick's law. Finally, the ideal selectivity of the separation of R-410A for each IL was calculated by taking the ratio of the Henry's law constants at 298.15 K and the ratio of the mass absorption at 1.0 MPa and 298.15 K.

2. MATERIALS AND METHODS

2.1. Materials. HFC-32 (CAS# 75-10-5) and HFC-125 (CAS# 354-33-6) were obtained from The Chemours Company (Newark, DE) with a minimum purity of 99.9 wt %, and used as received. ILs were purchased from commercial suppliers as follows: $[C_4C_1\text{im}][C_1CO_2]$ (assay, \geq 95 wt %, CAS

Table 1. HFC Critical Parameters

compound	$T_{\rm C}$ (K)	$P_{\rm C}~({\rm kPa})$	$eta_{ ext{HFC,A}}$	$eta_{ ext{HFC,B}}$	$eta_{ ext{HFC,C}}$	$eta_{ ext{HFC,D}}$
HFC-32	351.26	5782	1.0019	0.48333	-0.07538	0.00673
HFC-125	339.19	3637	1.0001	0.47736	-0.01977	-0.0177

no. 284049-75-8, Lot and Filling Code S25803 444041302), $[C_4C_1\text{im}][BF_4]$ (assay, ≥ 97 wt %, CAS no. 174501-65-6, Lot and Filling Code no. 1116280 23404335), [C₄C₁im][PF₆] (assay, ≥96 wt %, CAS no. 174501-64-5, Lot and Filling Code no. 1242554 304070904), $[C_4C_1 \text{im}][SCN]$ (assay, ≥ 95 wt %, CAS no. 344790-87-0, Lot and Filling code, S25812 14804B3), and $[C_6C_1\text{im}][Cl]$ (assay, ≥ 97 wt %, CAS no. 171058-17-6, Lot and Filling code, 1086333 41705081) were obtained from the Fluka Chemika (Switzerland). The [C₆C₁im][FAP] (assay, ≥99 wt %, CAS no. 713512-19-7, Lot and Filling code, S4872378 733) was purchased from EMD Millipore, Inc. (United States). The densities of HFC-32 and HFC-125 were obtained from the National Institute of Standards and Technology (NIST) REFPROP V.10.0 database.²¹ The densities and molecular weight of the ILs were obtained from the literature. 13,22 Figure 1 provides the chemical structures and acronyms for the HFC refrigerants and ILs studied in this work.

2.2. Experimental Methodology. The gas absorption measurements were performed using a gravimetric microbalance (Hiden Isochema Ltd., IGA 003, Warrington, United Kingdom). The experimental equipment and protocols for the gas solubility measurements have been described in detail in a prior reference; therefore, only a brief description is provided here. 13 Approximately 50 mg of IL was loaded in a flat bottom Pyrex sample container and degassed under vacuum (10⁻¹⁰ MPa) at 348.15 K for 12 h to remove any trace amounts of water and/or other volatile impurities prior to the measurements. The water content in the halogen-containing ILs was estimated to be less than 100 ppm and in the acetatecontaining IL to be less than 1000 ppm after in situ pretreatment. This estimation was validated by pulling a comparable vacuum on select IL samples using a Schlenk line and then analyzing them using a coulometric Karl Fisher titration method. Note that it has been demonstrated that [PF₆] and [BF₄] anions are hydrolytically unstable at elevated temperatures.²³ However, because the application under investigation involves moderate temperatures and the HFCs can be scrupulously dried, the [PF₆] and [BF₄] anions have demonstrated good stability. To ensure enough time to reach vapor-liquid equilibrium at 298.15 K, each pressure setpoint was held for a minimum of 8 h. The kinetic sorption profile and balance stability were monitored using the HISorp software program to ensure that the HFC/IL mixtures had reached thermodynamic equilibrium. The gas sorption measurements were performed in "static mode", where set point pressures were maintained constant within the system through simultaneous adjustments in admit and exhaust valves. The sample and counterweight temperatures were measured using an in situ K-type thermocouple with an uncertainty of ±0.1 K. Both temperature and pressure transducers in the microbalance were calibrated using NIST-certified reference instruments. The in situ thermocouple was calibrated using a standard platinum resistance thermometer (Hart Scientific SPRT model 5699 and readout Hart Scientific Blackstack model 1560 with a SPRT module 2560) with an accuracy of ± 0.005 K. Pressures under vacuum (10^{-10} to 10^{-5} MPa) were

measured using a Pfeiffer vacuum gauge (model PKR251) and pressures from vacuum (10^{-9} MPa) to higher pressure (2.0 MPa) were measured using a Druck pressure transducer (model PDCR4010) with an accuracy of ± 0.0008 MPa. The IGA microbalance had a mass resolution of 0.0001 mg for absorption and desorption measurements at any given temperature and pressure. The gas sorption data were corrected for buoyancy and volume expansion as described previously by Minnick et al.²⁴ Previous measurements for HFC-32 in $[C_4C_1\text{im}][PF_6]$ and $[C_4C_1\text{im}][BF_4]$ and HFC-125 in $[C_4C_1\text{im}][PF_6]$ were repeated to ensure that the new experimental setup being used for this study was able to reproduce the previous work (see the Supporting Information).

2.3. Equation of State Modeling. Solubilities of gases including HFCs in ILs have been accurately modeled using cubic EoS models as well as activity coefficient models, including NRTL, Wilson, and Margules. ^{19,22,25–34} To utilize experimental or computed solubility data in a process optimization framework, it is necessary to have analytic equations to represent the data. A particularly effective way of representing HFC/IL solubility data is with a cubic EoS. In 2010, Yokozeki and Shiflett showed a generic van der Waals EoS could accurately predict solubilities of gases including CO₂, NH₃, SO₂, and HFCs such as HFC-134a in ILs. ³⁵ In this work, parameters have been fit to the same generic van der Waals model for mixtures of HFC-32 and HFC-125 in the ILs studied. The van der Waals EoS is modeled by the equation:

$$P = \frac{RT}{V - b} - \frac{a(T)}{V^2} \tag{1}$$

$$a_i(T) = \frac{0.421875R^2 T_{ci}^2 \alpha_i(T)}{P_{ci}}$$
(2)

$$b_{i} = \frac{0.125RT_{ci}}{P_{ci}} \tag{3}$$

$$\alpha_{i}(T) = \sum_{k=0}^{\leq 3} \beta_{i,k} \left(\frac{1}{T_{ri}} - T_{ri} \right)^{k}, \qquad \left(T_{ri} \equiv \frac{T}{T_{ci}} \right)$$
(4)

where α represents the temperature dependence of the a parameter. The critical constant, β , the critical temperature, T_{cr} and the critical pressure, P_{cr} for HFC-32 and HFC-125 were obtained from prior calculations by Yokozeki³⁶ and are shown in Table 1.

Yokozeki proposed the following temperature dependence for the a parameter for ${\rm ILs}^{36}$

$$\alpha(T) = 1 + \beta_{\text{IL}} \left(\frac{1}{T_{\text{r,IL}}} - T_{\text{r,IL}} \right)$$
(5)

where $\beta_{\rm IL}$ is an adjustable fitting parameter and calculated for each IL. In this work, the $T_{\rm c}$ and $P_{\rm c}$ used for all ILs were set to 1000 K and 2.5 MPa, respectively. The model fit is extremely insensitive to the choice of IL $T_{\rm c}$ and $P_{\rm c}$ as shown in Section 3.

The following mixing rules were originally developed for refrigerant-lubricant mixtures involving large molecular-size differences and/or asymmetric interactions with respect to compositions and were extended to refrigerant/IL mixtures: 35,36

$$a = \sum_{i,j=1}^{N} \sqrt{a_i a_j} f_{ij}(T) (1 - k_{ij}) x_i x_j$$
(6)

$$f_{ij}(T) = 1 + \frac{\tau_{ij}}{T} \tag{7}$$

$$k_{ij} = \frac{l_{ij}l_{ji}(x_i + x_j)}{l_{ji}x_i + l_{ij}x_j}, \quad \text{where } k_{ii} = 0$$
(8)

$$b = 0.5 \sum_{i,j=1}^{N} (b_i + b_j)(1 - k_{ij})(1 - m_{ij})x_i x_j$$
(9)

Here l, m, and τ are binary interaction parameters, x_i is the mole fraction of species i, and R is the universal gas constant. We assume $l_{ii} = l_{jj} = 1$, $m_{ij} = m_{ji}$ and $m_{ii} = 0$, and $\tau_{ij} = \tau_{ji}$ and $\tau_{ii} = 0$, which leaves only four of these parameters $(l_{ij}, l_{ji}, m_{ij}, \text{ and } \tau_{ij})$ to be estimated via nonlinear regression. These simplifying assumptions are consistent with previous generic van der Waals EoS model calculations by Yokozeki and Shiflett. 35,36

With $\beta_{\rm IL}$ and the four binary interaction parameters, five total parameters were fit in this model. Many combinations of the parameters l_{ij} , l_{ji} m, τ , and $\beta_{\rm IL}$ are possible for which the model predictions closely match the experimental data; therefore, the choice of binary interaction parameters has negligible impact on the quality of the fit.

The fugacity coefficient is defined as

$$\ln \phi_{i} = \ln \left(\frac{RT}{P(V-b)} \right) + \frac{b'_{i}}{V-b} - \frac{a'_{i} + a}{VRT}$$
 (10)

where,

$$a_{i}' = 2\sum_{j=1}^{N} \sqrt{a_{i}a_{j}} f_{ij} x_{j} \left\{ 1 - k_{ij} - \frac{l_{ij}l_{ji}(l_{ij} - l_{ji})x_{i}x_{j}}{(l_{ji}x_{i} + l_{ij}x_{j})^{2}} \right\} - a$$
(11)

$$b_{i}' = \sum_{j=1}^{N} (b_{i} + b_{j})(1 - m_{ij})x_{j} \left\{ 1 - k_{ij} - \frac{l_{ij}l_{ji}(l_{ij} - l_{ji})x_{i}x_{j}}{(l_{ji}x_{i} + l_{ij}x_{j})^{2}} \right\}$$

$$- b \qquad (12)$$

and equilibria between the liquid and vapor phases is determined by

$$(x_i \phi_i)^{L} = (y_i \phi_i)^{V} \tag{13}$$

The amount of IL in the vapor phase is assumed to be zero because of the negligible vapor pressure of ILs; therefore, the vapor mole fraction of HFC is unity $(y_{HFC} = 1)$ and its phase equilibria are modeled by:

$$x_{\rm HFC}\phi_{\rm HFC}^{\rm L} = \phi_{\rm HFC}^{\rm V} \tag{14}$$

To fit the IL critical parameter and binary interaction parameters for each mixture, nonlinear regression was used to solve the following

$$\min_{l_{ij},l_{ji},m,\tau,\beta_{\rm IL}} (P_{\rm vdW} - P_{\rm exp})^2 \tag{15}$$

constrained by eqs 1-14 to calculate $P_{\rm vdW}$. $P_{\rm exp}$ are the experimentally measured pressures at equilibrium.

2.4. Henry's Law Constant at Infinite Dilution. Henry's law constants $(k_{\rm H})$ were used to evaluate the refrigerant absorption in ILs at infinite dilution concentrations, where lower $k_{\rm H}$ values indicate higher refrigerant solubility in the solvent.³⁷ In this work, both HFC-32 and HFC-125 solubilities increase linearly with increasing pressure up to about 0.2 MPa, indicating the Henry's law regime; therefore, the refrigerant partial pressure was directly proportional to its liquid composition in the liquid phase, under dilute conditions. The Henry's law constant can be calculated from experimental refrigerant solubility (PTx) data, assuming the hydrostatic pressure correction (Krichevsky–Kasarnovsky equation) is not required:

$$k_{\rm H} = \lim_{x_1 \to 0} \frac{f_1^{\rm V}(T, P, y_1)}{x_1} \approx \left(\frac{\mathrm{d}f_1^{\rm V}}{\mathrm{d}x_1}\right)_{x_1 = 0}$$
 (16)

where f_1^N is the vapor phase fugacity of HFC-32 and HFC-125 $(y_1 = 1)$ absorbed in the IL, which was calculated using an EoS model at given temperature and pressure. The Henry's law constants were calculated by determining the slope of a linear regression, fitting the experimental solubility data up to about 0.2 MPa, including the theoretical point with no refrigerant in the IL at zero pressure.

2.5. Fickian Diffusion Analysis. In addition to the equilibrium solubility, the time-dependent absorption data for HFC-32 and HFC-125 in the ILs were also measured using the gravimetric microbalance at 298.15 K and pressures ranging from 0.05 to 1.0 MPa. Details on how to apply Fick's law to the current physical situation have been previously reported; therefore, only a few important assumptions and conditions will be provided here.²⁸ In this simplified Fickian diffusion model, the following assumptions for the dissolving refrigerant in IL were applied: 13 (i) the interactions between the HFC and IL are physical; (ii) HFC dissolves through a one-dimensional (vertical) diffusion process, and there is no convective flow in the IL; (iii) a thin boundary layer exists between HFC and IL at given T and P, where thermodynamic equilibrium is established with the saturation concentration (C_s) ; (iv) HFC/IL mixture is a dilute solution, and thermophysical properties do not change at given T and P. These assumptions allow describing the dissolution of the HFC in ILs based on the one-dimensional mass diffusion because of local concentration difference

$$\frac{\partial C}{\partial t} = D \frac{\partial^2 C}{\partial z^2} \tag{17}$$

Initial condition

$$t = 0, \ 0 < z < L, \ \text{and} \ C = C_0$$
 (18)

Boundary conditions (i and ii)

(i)
$$t > 0$$
, $z = 0$, and $C = C_s$ (19)

(ii)
$$t > 0$$
, $z = L$, and $\frac{\partial C}{\partial z} = 0$ (20)

where C is the concentration of the HFC in the IL as a function of time (t), z is the vertical location, z=0

corresponds to the vapor—liquid boundary, L is the depth of the IL in the sample container, and D is the diffusion coefficient that was assumed to be constant. The depth (L) was estimated by knowing the cylindrical geometry of the sample container, mass, and average weight fraction density of the HFC/IL mixture at initial (C_0) and saturation concentration (C_s) at a given T and P. Equation 17 was solved analytically by applying the proper initial and boundary conditions (eqs 18–20), and the separation of variables or Laplace transform methods to yield the following 38

$$\langle C \rangle = C_{\rm s} \left[1 - 2 \left(1 - \frac{C_0}{C_{\rm s}} \right) \sum_{n=0}^{\infty} \frac{\exp(-\lambda_n^2 Dt)}{L^2 \lambda_n^2} \right]$$
 (21)

where $\lambda_n = [n + (1/2)](\pi/L)$.

Although eq 21 has an infinite summation term, only the first ten terms were applied in this analysis. The diffusion coefficient (D) and solubility limit at equilibrium (C_s) for each HFC in IL data set were calculated through nonlinear regression of eq 21 using MATLAB software, and the best model fit was obtained by selecting the proper C_0 value (see the Supporting Information for additional details).

3. RESULTS AND DISCUSSION

3.1. Vapor Liquid Equilibrium Results. Previous studies indicate that the HFC solubility in ILs depends primarily on

Table 2. Experimental VLE for HFC-32/ $[C_4C_1im][BF_4]$ and HFC-125/ $[C_4C_1im][BF_4]$ Mixtures at 298.15 K^a

HFC-32 (1) + $[C_4C_1im][BF_4]$ (2)			HFC-125 (1) + $[C_4C_1im][BF_4]$ (2)		
P (MPa)	100x ₁ (mol %)	(wt %)	P (MPa)	100x ₁ (mol %)	(wt %)
0.05	2.4	0.6	0.05	0.8	0.4
0.1	5.8	1.4	0.1	1.9	1.0
0.2	12.2	3.1	0.2	4.3	2.3
0.4	23.9	6.8	0.4	10.1	5.6
0.6	36.5	11.8	0.6	17.2	10.0
0.8	44.6	15.8	0.8	26.3	15.9
1.0	54.5	21.9	1.0	37.8	24.4

^aP—pressure; $100x_1$ and w_1 —HFC composition (wt %) in IL. Standard uncertainties: u(T)=0.1 °C; u(P)=0.0008 MPa and $u(100x_1)=0.5$ mol %.

Table 3. Experimental VLE for HFC-32/ $[C_4C_1\text{im}][PF_6]$ and HFC-125/ $[C_4C_1\text{im}][PF_6]$ Mixtures at 298.15 K^a

HFC-32 (1) + $[C_4C_1\text{im}][PF_6]$ (2)			HFC-125 ($(1) + [C_4C_1 im$	$[PF_6](2)$
P (MPa)	100x ₁ (mol %)	(wt %)	P (MPa)	100x ₁ (mol %)	(wt %)
0.05	3.9	0.7	0.05	1.2	0.5
0.1	7.6	1.5	0.1	2.4	1.0
0.2	14.6	3.0	0.2	4.8	2.1
0.4	27.3	6.4	0.4	9.9	4.4
0.6	38.4	10.2	0.6	16.0	7.2
0.8	48.3	14.6	0.8	23.2	11.0
1.0	57.4	19.8	1.0	32.3	16.1

^aP—pressure; $100x_1$ and w_1 —HFC composition (wt %) in IL. Standard uncertainties: u(T) = 0.1 °C; u(P) = 0.0008 MPa and $u(100x_1) = 0.5$ mol %.

the interaction strength between the refrigerant and the IL anion.³⁹ For instance, Shiflett and Yokozeki reported that

Table 4. Experimental VLE for HFC-32/ $[C_6C_1\text{im}][FAP]$ and HFC-125/ $[C_6C_1\text{im}][FAP]$ Mixtures at 298.15 K^a

HFC-32 (1) + $[C_6C_1im][FAP]$ (2)			$HFC-125 (1) + [C_6C_1im][FAP] (2)$		
P (MPa)	100x ₁ (mol %)	(wt %)	P (MPa)	100x ₁ (mol %)	(wt %)
0.05	6.7	0.6	0.05	3.8	0.8
0.1	12.6	1.2	0.1	7.4	1.5
0.2	23.3	2.5	0.2	14.2	3.1
0.4	40.2	5.4	0.4	26.7	6.6
0.6	53.1	8.8	0.6	38.0	10.7
0.8	63.4	12.9	0.8	48.2	15.3
1.0	72.0	18.1	1.0	57.8	20.9

^aP—pressure; $100x_1$ and w_1 —HFC composition (wt %) in IL. Standard uncertainties: u(T) = 0.1 °C; u(P) = 0.0008 MPa and $u(100x_1) = 0.5$ mol %.

Table 5. Experimental VLE for HFC-32/ $[C_4C_1\text{im}][C_1\text{CO}_2]$ and HFC-125/ $[C_4C_1\text{im}][C_1\text{CO}_2]$ Mixtures at 298.15 K^a

HFC-32 (1) + $[C_4C_1im]$ $[C_1CO_2]$ (2)			HFC-125 (1) + $[C_4C_1im]$ $[C_1CO_2]$ (2)			
P (MPa)	100x ₁ (mol %)	(wt %)	P (MPa)	100x ₁ (mol %)	(wt %)	
0.05	5.4	1.5	0.05	6.0	3.7	
0.1	9.7	2.7	0.1	12.2	7.7	
0.2	16.1	4.8	0.2	24.0	16.0	
0.4	26.8	8.7	0.4	42.9	31.0	
0.6	35.7	12.6	0.6	53.6	40.8	
0.8	43.8	16.8	0.8	62.0	49.1	
1.0	51.0	21.2	1.0	69.2	56.9	

^aP—pressure; $100x_1$ and w_1 —HFC composition (wt %) in IL. Standard uncertainties: u(T) = 0.1 °C; u(P) = 0.0008 MPa and $u(100x_1) = 0.5$ mol %.

Table 6. Experimental VLE for HFC-32/ $[C_4C_1\text{im}][SCN]$ and HFC-125/ $[C_4C_1\text{im}][SCN]$ Mixtures at 298.15 K^a

HFC-32 (1) + $[C_4C_1im][SCN]$ (2)			HFC-125 (1) + $[C_4C_1\text{im}][SCN]$ (2)			
P (MPa)	100x ₁ (mol %)	(wt %)	P (MPa)	100x ₁ (mol %)	(wt %)	
0.05	0.4	0.1	0.05	<0.1	<0.1	
0.1	2.4	0.6	0.1	0.4	0.3	
0.2	5.7	1.6	0.2	1.3	0.8	
0.4	12.7	3.7	0.4	3.1	1.9	
0.6	21.2	6.6	0.6	5.3	3.2	
0.8	28.0	9.3	0.8	7.7	4.7	
1.0	34.9	12.4	1.0	10.5	6.5	

"P—pressure; $100x_1$ and w_1 —HFC composition (wt %) in IL. Standard uncertainties: u(T)=0.1 °C; u(P)=0.0008 MPa and $u(100x_1)=0.5$ mol %.

HFC-32 is more soluble in ILs containing fluorinated anions than in those with non-fluorinated anions because of hydrogen bonding between the hydrogen on the refrigerant and the fluorine on the anion. ²⁸ In addition, the same authors found large solubility differences for HFC-32 relative to HFC-125 in $[C_4C_1\text{im}][PF_6]$. For example, HFC-32/ $[C_4C_1\text{im}][PF_6]$ had a Henry's law constant of 8.8 \pm 0.7 bar, while HFC-125/ $[C_4C_1\text{im}][PF_6]$ had a Henry's law constant of 23.1 \pm 2.3 bar at 298.15 K. ¹³ To validate this theory, experimental solubility data of HFC-32 and HFC-125 in three ILs with fluorinated anions ($[C_4C_1\text{im}][BF_4]$, $[C_4C_1\text{im}][PF_6]$, and $[C_6C_1\text{im}][FAP]$) and in three ILs with non-fluorinated anions

Table 7. Experimental VLE for HFC-32/ $[C_6C_1\text{im}][Cl]$ and HFC-125/ $[C_6C_1\text{im}][Cl]$ Mixtures at 298.15 K^a

HFC-32 (1) + $[C_6C_1im][Cl]$ (2)			HFC-125 (1) + $[C_6C_1im][Cl]$ (2)		
P (MPa)	100x ₁ (mol %)	(wt %)	P (MPa)	100x ₁ (mol %)	(wt %)
0.05	2.1	0.5	0.05	4.0	2.4
0.1	4.4	1.2	0.1	7.9	4.8
0.2	9.2	2.5	0.2	16.0	10.2
0.4	18.6	5.6	0.4	29.0	19.5
0.6	27.2	8.8	0.6	41.4	29.6
0.8	34.5	11.9	0.8	54.3	41.3
1.0	41.0	15.2	1.0	65.4	52.8

^aP—pressure; $100x_1$ and w_1 —HFC composition (wt %) in IL. Standard uncertainties: u(T) = 0.1 °C; u(P) = 0.0008 MPa and $u(100x_1) = 0.5$ mol %.

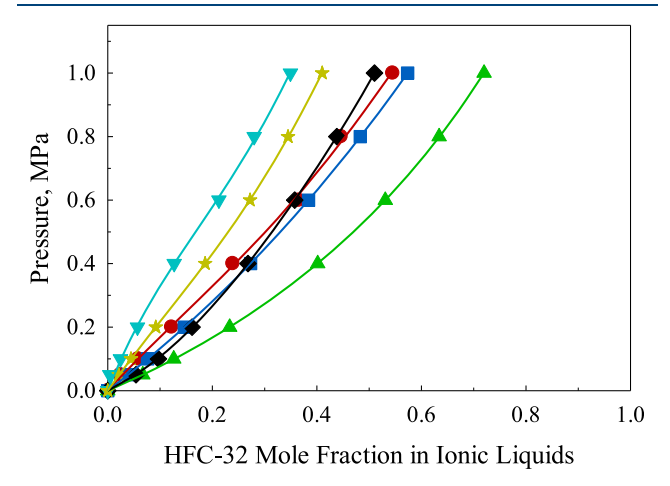


Figure 2. VLE for HFC-32 in $[C_4C_1im][SCN]$ (▼), $[C_6C_1im][Cl]$ (★), $[C_4C_1im][C_1CO_2]$ (♦), $[C_4C_1im][BF_4]$ (●), $[C_4C_1im][PF_6]$ (■), and $[C_6C_1im][FAP]$ (▲) at 298.15 K. Symbols are measured experimental data (PTx) and lines are van der Waals EoS model predictions.

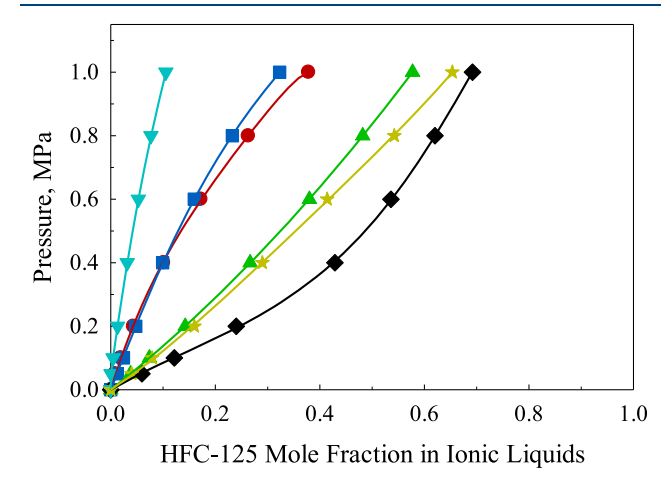


Figure 3. VLE for HFC-125 in $[C_4C_1\text{im}][SCN]$ (\blacktriangledown), $[C_4C_1\text{im}][PF_6]$ (\blacksquare), $[C_4C_1\text{im}][BF_4]$ (\bullet), $[C_6C_1\text{im}][FAP]$ (\blacktriangle), $[C_6C_1\text{im}][Cl]$ (\bigstar), and $[C_4C_1\text{im}][C_1CO_2]$ (\spadesuit) at 298.15 K. Symbols are measured experimental data (PTx), and solid lines are van der Waals EoS model predictions.

($[C_4C_1im][C_1CO_2]$, $[C_4C_1im][SCN]$, and $[C_6C_1im][Cl]$) at pressures ranging from 0.05 to 1.0 MPa and at 298.15 K were

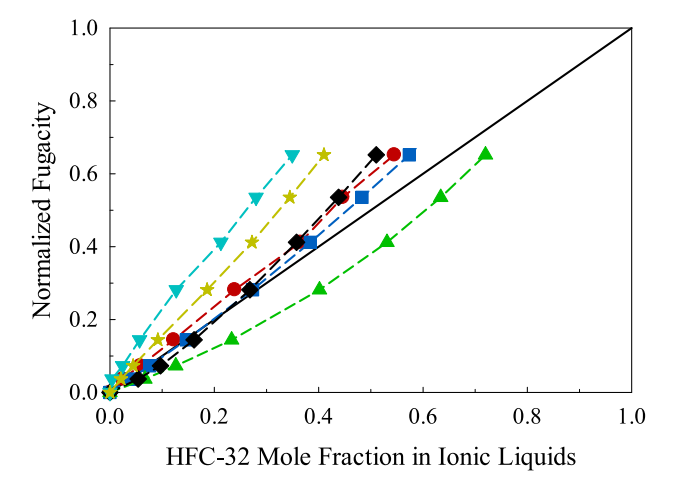


Figure 4. Normalized fugacity for HFC-32 in $[C_4C_1\text{im}][SCN]$ (\blacktriangledown), $[C_6C_1\text{im}][Cl]$ (\bigstar), $[C_4C_1\text{im}][C_1CO_2]$ (\spadesuit), $[C_4C_1\text{im}][BF_4]$ (\spadesuit), $[C_4C_1\text{im}][PF_6]$ (\blacksquare), and $[C_6C_1\text{im}][FAP]$ (\blacktriangle) as a function of refrigerant molar composition at 298.15 K. Solid line represents Raoult's law. Dashed lines were added as a guide for the reader.

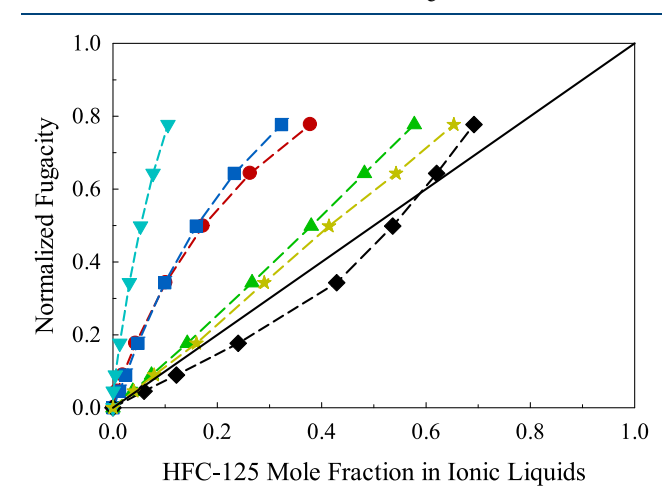


Figure 5. Normalized fugacity for HFC-125 in $[C_4C_1\mathrm{im}][SCN]$ (♥), $[C_4C_1\mathrm{im}][PF_6]$ (■), $[C_4C_1\mathrm{im}][BF_4]$ (●), $[C_6C_1\mathrm{im}][FAP]$ (♠), $[C_6C_1\mathrm{im}][Cl]$ (★), and $[C_4C_1\mathrm{im}][C_1CO_2]$ (♦) as a function of refrigerant molar composition at 298.15 K. Solid line represents Raoult's law. Dashed lines were added as a guide for the reader.

Table 8. van der Waals EoS Model Parameters for HFC-32

		HFC-32/IL van der Waals parameters						
IL	l_{ij}	l_{ji}	m	τ	$eta_{ ext{IL}}$			
[C ₆ C ₁ im] [FAP]	0.76263	0.76227	-3.1790	1070.6	0.80407			
$\begin{bmatrix} C_4C_1im \\ BF_4 \end{bmatrix}$	0.84646	0.84015	-5.2491	1492.4	0.25646			
$\begin{bmatrix} C_4C_1im \\ PF_6 \end{bmatrix}$	0.77015	0.76988	-3.3283	1079.2	0.96279			
$\begin{bmatrix} C_4 C_1 im \\ [C_1 CO_2] \end{bmatrix}$	0.68425	0.68604	-2.1789	1152.3	4.9624			
$\begin{bmatrix} C_6 C_1 im \\ Cl \end{bmatrix}$	0.86666	0.85663	-5.8300	1500.0	0.24679			
$\begin{bmatrix} C_4C_1im \\ SCN \end{bmatrix}$	0.90109	0.87156	-6.72538	1499.8	0.033817			

measured (Tables 2-7) and correlated using the van der Waals EoS model as shown in Figures 2 and 3.

It is worth mentioning that the absorption equilibrium isotherms shown in Figures 2 and 3 were measured up to 1.0

Table 9. van der Waals EoS Model Parameters for HFC-125

	HFC-125/IL van der Waals parameters						
IL	l_{ij}	l_{ji}	m	τ	$eta_{ ext{IL}}$		
$\begin{bmatrix} C_6 C_1 im \\ [FAP] \end{bmatrix}$	0.75724	0.75777	-3.1236	1096.9	0.84396		
$\begin{bmatrix} C_4 C_1 im \\ BF_4 \end{bmatrix}$	0.94755	0.88067	-9.7377	1495.6	-0.19398		
$\begin{bmatrix} C_4C_1im \\ PF_6 \end{bmatrix}$	0.63148	0.63317	-1.7454	1187.0	4.9560		
$ \begin{bmatrix} C_4C_1im \end{bmatrix}[\\ C_1CO_2 \end{bmatrix}$	0.40726	0.24824	-0.34565	115.93	0.053203		
$\begin{bmatrix} C_6 C_1 im \end{bmatrix}$ $\begin{bmatrix} Cl \end{bmatrix}$	0.79991	0.80272	-4.0687	1440.3	0.83820		
$\begin{bmatrix} C_4 C_1 im \\ SCN \end{bmatrix}$	0.96174	0.92967	-9.9840	1.6323	0.75431		

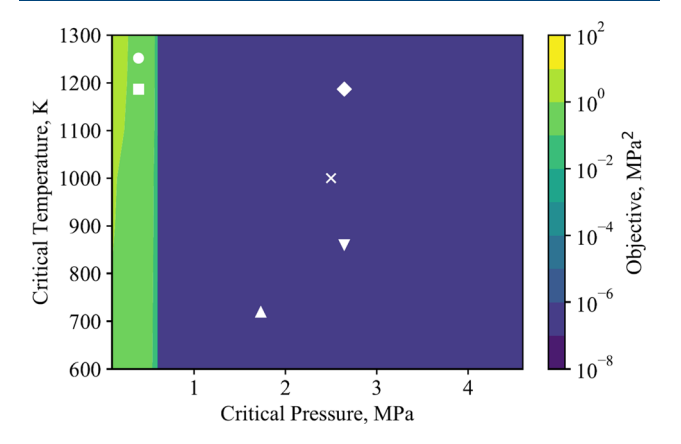


Figure 6. Critical temperature and pressure sensitivity analysis for the solubility of HFC-32 in the IL $[C_4C_1 \text{im}][PF_6]$. The markers indicate critical temperatures and pressures calculated by: Vetere's Method³⁵ (\blacktriangledown), Gibbs ensemble Monte Carlo⁴⁴ (\bullet), surface tension-based empirical equations to calculate critical temperature and Vetere's method critical pressure ^{35,43} (\bullet), surface tension-based empirical equations to calculate critical temperature and Gibbs ensemble Monte Carlo critical pressure ^{43,44} (\blacksquare), and group contribution methods⁴⁵ (\blacktriangle). The x marker indicates the critical temperature and pressure values used in this work.

MPa in order to not exceed the saturation vapor pressure at 298.15 K of the HFCs studied in this work , that is, 1.69 and 1.38 MPa for HFC-32 and HFC-125, respectively. 21

To validate the experimental method and general solubility trends reported in this work, the solubility data for HFC-32 and HFC-125 in fluorinated and nonfluorinated anion-based ILs were compared with those reported in the literature. In general, the experimental VLE data obtained are in good agreement with previous reports (Figures S1–S3). For example, the solubility data for HFC-32 and HFC-125 in $[C_4C_1\mathrm{im}][PF_6]$ and $[C_4C_1\mathrm{im}][BF_4]$ are on average within 0.6–2.8 mol % of those data reported by Shiflett and Yokozeki in 2006.

As expected, the solubility of HFC-32 and HFC-125 increase with increasing pressure for any given IL. However, it is the relative differences in solubility for either HFC-32 or HFC-125 that is most important, particularly for selective separation of R410A. For example, HFC-32 is 44.2% (mole fraction basis) more soluble than HFC-125 in $[C_4C_1\text{im}][BF_4]$ at 298.15 K and 1.0 MPa. A similar trend was obtained by Liu et al., who found that HFC-32 is more soluble than HFC-125 in $[C_6C_1\text{im}][NTf_2]$ at a given temperature and pressure. However, the more important comparison for designing

separation systems is the difference in solubility based on a mass fraction basis. In this case, because of molecular weight differences (HFC-32 MW = 52.024 g·mol⁻¹ and HFC-125 MW = 120.02 g·mol⁻¹), the HFC-125 is only 11.4% more soluble than HFC-32 at 298.15 K and 1.0 MPa. Similar differences in solubility were found for the other ILs with fluorinated anions, $[C_4C_1\text{im}][PF_6]$ and $[C_6C_1\text{im}][FAP]$, as shown in Tables 3 and 4, respectively.

In addition to the anion fluorination of the imidazolium-based ILs, a longer alkyl chain length for the cation may play a role in increasing the HFC-32 and HFC-125 absorption in the $[C_6C_1\mathrm{im}][FAP]$ IL. For example, comparing HFC-134a solubility in various ILs at 298.15 K, it is clear that a longer alkyl chain on the cation increases the absorption of HFC-134a, as lower HFC-134a solubility was observed in $[C_2C_1\mathrm{im}][NTf_2]$ relative to $[C_6C_1\mathrm{im}][NTf_2]^{.39}$ Moreover, Shiflett et al. found higher HFC-32 solubilities in $[C_6C_1\mathrm{im}][TFES]$ relative to $[C_4C_1\mathrm{im}][TFES]^{.40}$ It is worth mentioning that IL cations with longer hydrogenated chains and/or anions with a larger number of fluorine atoms have been associated with increasing levels of IL toxicity.

3.2. Deviation from Ideality (Raoult's Law). To evaluate the nonideality of HFC-32 and HFC-125 in IL, the normalized fugacity as a function of HFC molar compositions in the liquid phase was evaluated. The normalized fugacity was expressed as $f^{\rm v}/f^{\rm at}$, where $f^{\rm v}$ refers to the vapor phase fugacity of the HFC resulting from the negligible vapor pressure of the IL, ⁴² such that $y_{\rm ref} = 1$, and $f^{\rm sat}$ corresponds to the fugacity of the HFC at saturated vapor pressure with a temperature of 298.15 K. Figures 4 and 5 show the normalized fugacity for HFC-32 and HFC-125 in the ILs studied in this work as a function of molar compositions at 298.15 K.

It is most interesting that these refrigerants within the same family of HFCs show quite distinct solubility behaviors depending on the choice of IL. For instance, HFC-32 had a strong negative deviation from Raoult's law in $[C_6C_1\text{im}][FAP]$ across the entire refrigerant composition range, suggesting that the phase behavior was dominated by stronger van der Waals interactions between HFC-32 and this IL. In addition, HFC-32 exhibited a nearly ideal solubility behavior in [C₄C₁im]-[C₁CO₂] and [C₄C₁im][PF₆] for lower refrigerant compositions (up to 0.3 mol fraction), whereas at higher refrigerant mole fractions, it showed a slightly positive deviation from Raoult's law. HFC-32 showed positive deviations over all compositions in $[C_4C_1im][SCN]$, $[C_4C_1im][BF_4]$, and [C₆C₁im][Cl]. Similar findings were obtained by Shiflett and Yokozeki, who found that HFC-32 exhibited negative and positive deviations from Raoult's law in ILs with fluorinated and nonfluorinated anions, respectively, depending on refrigerant composition. 13 The strong absorption mechanism for HFC-32 in ILs with fluorinated anions has been proposed to be because of hydrogen bonding between the electronegative fluorinated IL anion (BF4, PF6, and FAP) and the acidic hydrogen atoms on the fluorocarbon (CH₂F₂).¹³ Unlike HFC-32, HFC-125 exhibited a strong positive deviation from Raoult's law in ILs with fluorinated anions (BF4, PF6, and FAP), which may indicate that the cohesive forces between HFC-125 and the IL are weaker than cohesive forces between HFC/HFC and/or IL/IL. Interestingly, HFC-125 in [C₄C₁im][C₁CO₂] showed mixed negative and positive deviations from Raoult's law, depending on the molar concentration of the refrigerant. For instance, HFC-125 exhibited negative deviation for lower refrigerant mole

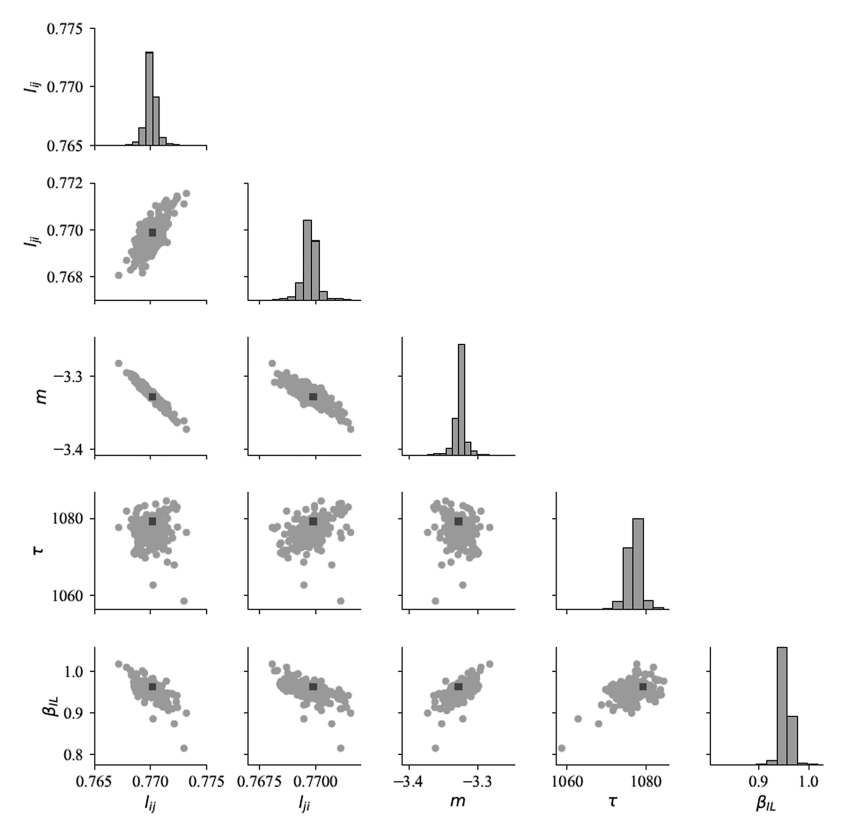


Figure 7. Uncertainty analysis of van der Waals EoS model parameters for the solubility of HFC-32 in $[C_4C_1\text{im}][PF_6]$. Histograms for each parameter are shown on the diagonal, depicting the variability of each parameter. Scatter plots below the diagonal show the pairwise variability of the fitted parameters, with the dark gray squares indicating the parameters calculated with the original dataset shown in Table 8.

Table 10. Henry's Law Constants (MPa) for HFC-32 and HFC-125 in ILs at 298.15 K^a

	Henry's law cons		
IL	HFC-32	HFC-125	selectivity S_{Hij}
$[C_4C_1im][BF_4]$	1.54 ± 0.06	4.19 ± 0.17	0.37
$[C_4C_1im][PF_6]$	1.34 ± 0.01	4.05 ± 0.06	0.33
$[C_6C_1im][FAP]$	0.84 ± 0.03	1.37 ± 0.01	0.61
$[C_4C_1im][C_1CO_2]$	1.20 ± 0.11	0.81 ± 0.00	1.48
$[C_4C_1im][SCN]$	3.11 ± 0.37	13.32 ± 2.44	0.23
$[C_6C_1im][Cl]$	2.00 ± 0.00	1.16 ± 0.03	1.72

^aThe uncertainties are the standard error of the coefficient obtained in the linear regression.

fractions (up to approximately 0.6), whereas, at higher refrigerant compositions, it showed positive deviation from Raoult's law. These results suggest that the carboxylate group in the IL anion plays an important role in increasing the solubility of HFC-125. Similar findings were reported by Sosa et al., who reported that HFC-125 is significantly more soluble than HFC-32 in [C₄C₁im][C₁CO₂] at 303.15 K and any given pressure. The excess Gibbs energy for HFC-32 and HFC-125 were calculated in each of the ILs and can be found in the Supporting Information (Figures S4 and S5). The differences in excess Gibbs energy for HFC-32 and HFC-125 for each IL correlate with the differences in solubility based on mole fraction. It is worth mentioning that molecular dynamics simulations and calorimetric studies are underway to fully understand the observed HFC solubility trends.

3.3. van der Waals EoS Modeling. Figures 2 and 3 show the van der Waals EoS model predictions for the solubilities of

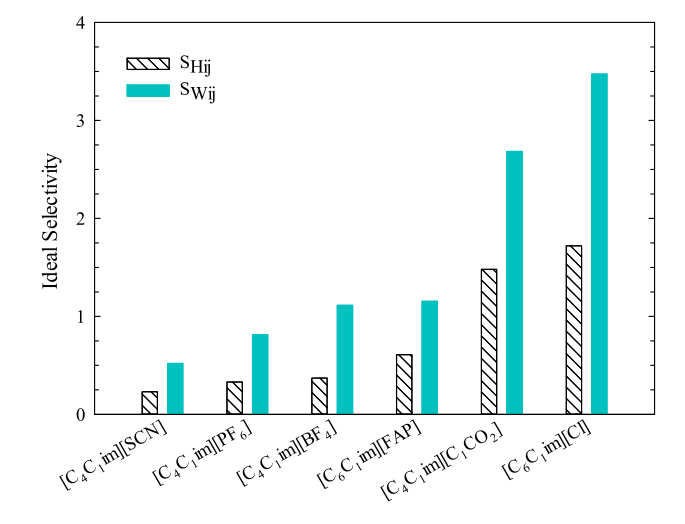


Figure 8. Ideal selectivity for the absorption of HFC-32 and HFC-125 in ILs. The ideal selectivity was calculated based on the ratio of the Henry's law constants ($S_{\rm Hij}$) in the ILs at 298.15 K and the ratio of the weight fractions ($S_{\rm Wij}$) in the ILs at 1.0 MPa and 298.15 K.

HFC-32 and HFC-125 in ILs using the best fit parameters reported in Tables 8 and 9, respectively.

These results are consistent with Yokozeki and Shiflett, 35 who show the van der Waals EoS model can accurately predict phase equilibria for HFC-134a and the IL $[C_2C_1\text{im}][Tf_2N]$ mixtures. However, there is no guarantee that the parameters presented in Tables 8 and 9 are at the global optimum because eq 15 is a nonconvex optimization problem, and there may exist other parameter values that give similar high-quality fits.

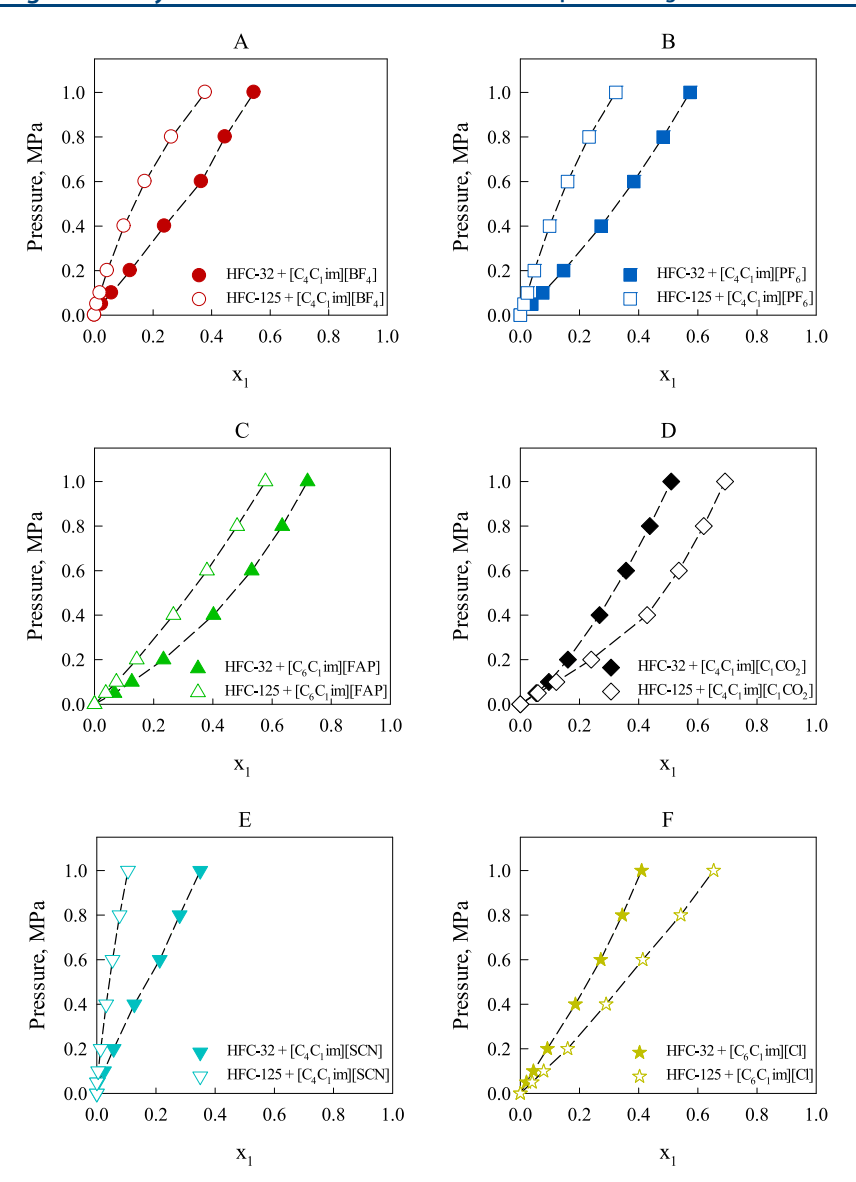


Figure 9. Comparison of HFC-32 and HFC-125 VLE (mol fraction, x_1) in ILs: (A) $[C_4C_1\text{im}][BF_4]$, (B) $[C_4C_1\text{im}][PF_6]$, (C) $[C_6C_1\text{im}][FAP]$, (D) $[C_4C_1\text{im}][C_1CO_2]$, (E) $[C_4C_1\text{im}][SCN]$, and (F) $[C_6C_1\text{im}][Cl]$ at 298.15 K.

Because ILs decompose before reaching their critical temperatures^{43,44} and actual critical points cannot be determined experimentally, hypothetical values (pseudocritical points) were used for ILs in this analysis. Multiple studies have sought to predict the pseudocritical points for ILs. For the IL [C₄C₁im][PF₆], pseudocritical property estimation methods include density and surface tension-based empirical equations, 43 group contribution methods, 45 Gibbs ensemble Monte Carlo, 44 and the critical-volume based Vetere's method. 55 However, these various methods result in estimates for [C₄C₁im][PF₆] pseudocritical temperatures and pressures ranging from 600 to 1300 K and 0.39 to 3.0 MPa, respectively. Previous analysis by Yokozeki and Shiflett suggested the generic van der Waals model was not sensitive to IL critical properties.^{35,36} To verify this, a systematic analysis of the model fit was performed, quantified by the sum of residuals squared, with respect to T_c from 600 to 1400 K and P_c from 0.1 MPa to 5.0 MPa for the mixture of HFC-32 in $[C_4C_1\text{im}][PF_6]$. The objective function is shown in Figure 6 as colored contours with respect to T_c and P_c , and the critical

points estimated by the methods listed above are marked by symbols. For $P_{\rm c}$ values below 0.5 MPa the objective function is on the order of 10^{-1} to 10^{1} , which indicates a poor fit of the experimental data. For $P_{\rm c}$ values greater than 0.5 MPa and all $T_{\rm c}$, the model returns feasible solutions with objective function values on the order of 10^{-6} . This indicates the van der Waals EoS model is insensitive to $T_{\rm c}$ and $P_{\rm c}$ for ILs; therefore, it is unnecessary to determine highly accurate IL pseudocritical properties when fitting the van der Waals EoS model parameters to binary mixture solubility data; any critical point estimate can be used if its critical pressure is greater than 0.5 MPa. As mentioned in Section 2.3, the $T_{\rm c}$ and $P_{\rm c}$ for each IL were set at 1000 K and 2.5 MPa, respectively. This is also likely true for other EoS models but should be tested.

Monte Carlo uncertainty analysis 46,47 was also performed for the fitted parameters of the mixture of HFC-32 in $[C_4C_1\text{im}]$ - $[PF_6]$. To summarize, normally distributed random error was added to the experimental x, T, and P in Table 3 to create a new "simulated" experimental dataset. The values of error were chosen to correspond with experimental precision for x, T, and

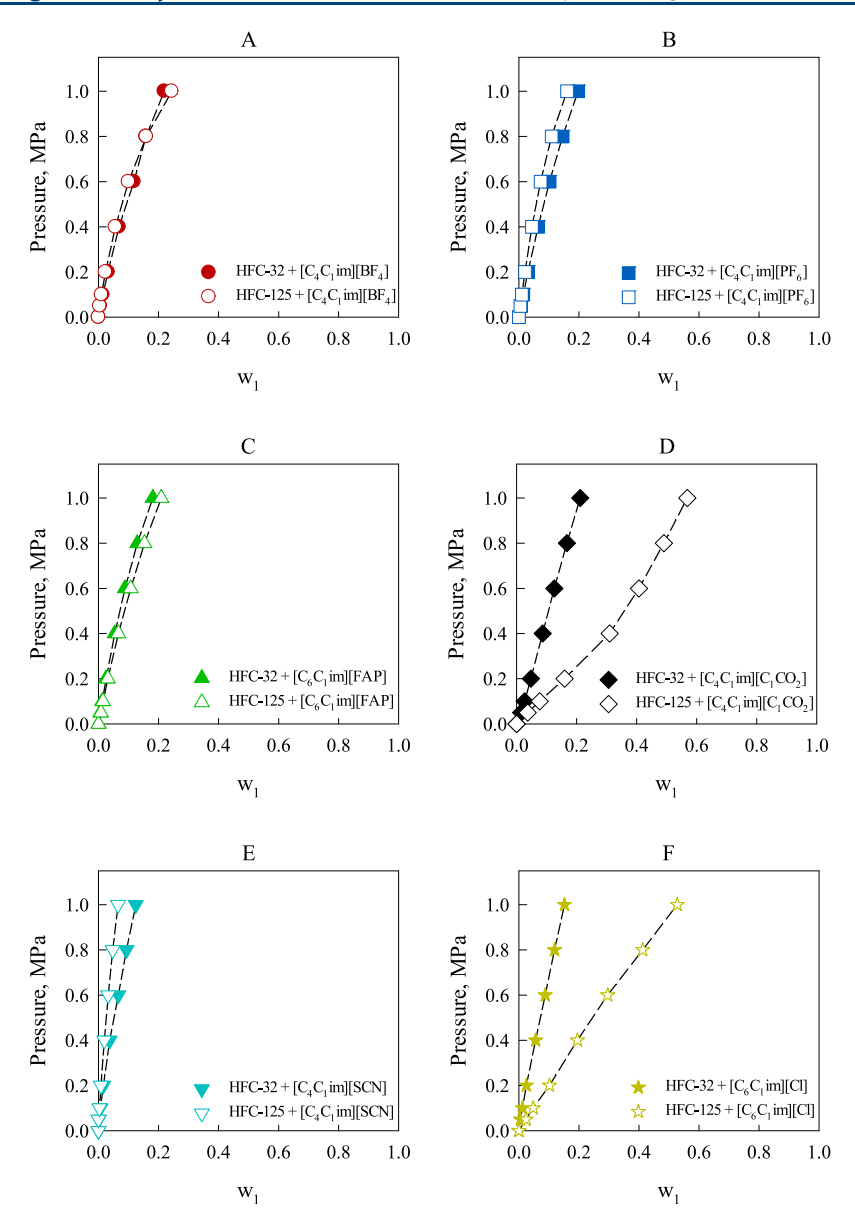


Figure 10. Comparison of HFC-32 and HFC-125 VLE (mass fraction, w_1) in ILs: (A) $[C_4C_1\text{im}][BF_4]$, (B) $[C_4C_1\text{im}][PF_6]$, (C) $[C_6C_1\text{im}][FAP]$, (D) $[C_4C_1\text{im}][C_1CO_2]$, (E) $[C_4C_1\text{im}][SCN]$, and (F) $[C_6C_1\text{im}][Cl]$ at 298.15 K.

Table 11. Estimated Fickian Diffusion Coefficients for HFC-32/IL and HFC-125/IL Systems at 298.15 K and 0.05 MPa and Reported Viscosities for ILs at 298.15 K and 0.1 MPa

		HFC-32 (1)/IL (2)		HFC-125 (1)/IL (2)	
IL	viscosity (Pa·s)	D (10 ⁻¹¹ m ² ·s ⁻¹)	C _s (wt %)	D (10 ⁻¹¹ m ² ·s ⁻¹)	C _s (wt %)
$[C_6C_1im][Cl]$	18.1 ± 1.8^{50}	1.5	0.5	0.4	3.2
$[C_4C_1im][C_1CO_2]$	0.448 ± 0.019^{52}	0.5	1.5	1.3	3.7
$[C_4C_1im][PF_6]$	0.271 ± 0.021^{53}	8.5	0.7	1.7	0.5
$[C_4C_1im][BF_4]$	0.1014 ± 0.0027^{54}	7.8	0.6	2.4	0.4
$[C_6C_1im][FAP]$	0.0882 ± 0.0021^{55}	19.6	0.6	5.5	0.8
$[C_4C_1\text{im}][SCN]$	0.0517 ± 0.00055^{56}	_	_	_	_

^aThe estimated diffusivity uncertainty was estimated to be within a factor of two in the calculated diffusivity. ¹³

P, and the normal distribution over which the errors were randomly chosen was located within each measurement's standard uncertainty: ± 0.005 (unitless) for mole fraction, ± 0.1 K for temperature, and ± 0.0008 MPa for pressure. Using the simulated data, the van der Waals parameters l_{ij} , l_{ji} m, τ , and $\beta_{\rm IL}$ were refit and the results recorded. This procedure was

repeated one thousand times. Thus, one thousand simulated experimental datasets, with x, T, and P values varying within the experimental precisions, were generated, and van der Waals parameters were fit to each simulated dataset. This provided a multivariate distribution of the fitted parameters, which is shown in Figure 7. The Monte Carlo procedure provides the

expected deviation in the fitted results if the experiments were repeated hundreds of times.

Three important insights about our experimental data and fitted model can be gained from Figure 7. The plots along the diagonal of Figure 7 are histograms for the five-fitted parameters. The first insight is that the parameter l_{ii} has a variability of 0.785%, l_{ii} has a variability of 0.454%, m has a variability of 2.66%, τ has a variability of 2.44%, and β_{II} has a variability of 25.0%. This variability is induced by random errors of similar magnitude to the experimental precision. In other words, a variability of at least this large is expected if the experiments were repeated with the same equipment. The variability of the fitted parameter $\beta_{\rm IL}$ is 1-2 orders of magnitude larger than the other parameters. This gives the second insight: $\beta_{\rm IL}$ is a sloppy parameter, 48 which means that it cannot be determined uniquely from these data. This is because the quality of fit (sum of residuals squared) is insensitive with respect to β_{II} . Scatter plots below the diagonal of Figure 7 show pairwise variability in the fitted parameters. The highest histogram bars (on the diagonal) correspond with the tightest clusters of parameters in the scatter plots (off the diagonal). The dark gray squares mark the parameter values for HFC-32 in [C₄C₁im][PF₆] reported in Table 8, which were calculated with the original experimental data from Table 3. In each scatter plot, this dark gray square is located in the densest regions of parameters. From these scatter plots, we get our third key insight: parameters l_{ii} , l_{ii} , m, and β_{II} are correlated. This suggests there exists an alternate thermodynamic model with one or fewer fitted parameters that gives a similar quality of fit (sum of residuals squared).

3.4. Ideal Selectivity Based on Henry's Law Constants. The most suitable IL for a specific gas separation process hinges on the gas absorption capacity, the ability to preferentially absorb one gas over another from a mixture, and the ability to facilitate gas diffusion (as discussed in Section 3.5). In this context, the ideal selectivity has been reported as a parameter to assess the ability of a given pure IL to separate HFC-32 and HFC-125 in R-410A. The ideal selectivity can be defined as the ratio of the Henry's law constants of the HFC refrigerants at a given temperature, as follows: ¹⁵

$$S_{\mathrm{H}ij} = \left(\frac{k_{\mathrm{H}i}}{k_{\mathrm{H}j}}\right)_{\mathrm{T}} \tag{22}$$

where $k_{\rm H\it{i}}$ and $k_{\rm H\it{j}}$ are the Henry's law constants calculated for the HFC refrigerants, i= HFC-32 and j= HFC-125, respectively.

Henry's law constants for HFC-32 and HFC-125 in the ILs were calculated using the method described in Section 2.5, and the results are summarized in Table 10.

Comparing the Henry's law constants calculated for HFC-32 in ILs at 298.15 K shows that $k_{\rm H}$ (MPa) follows the order: $[{\rm C_6C_1im}][{\rm FAP}] < [{\rm C_4C_1im}][{\rm C_1CO_2}] < [{\rm C_4C_1im}][{\rm PF_6}] < [{\rm C_4C_1im}][{\rm BF_4}] < [{\rm C_6C_1im}][{\rm Cl}] < [{\rm C_4C_1im}][{\rm SCN}]$, which is in good agreement with the general solubility trends reported in Tables 2–7 On the other hand, HFC-125 $k_{\rm H}$ (MPa) follows the order: $[{\rm C_4C_1im}][{\rm C_1CO_2}] < [{\rm C_6C_1im}][{\rm Cl}] < [{\rm C_6C_1im}][{\rm FAP}] < [{\rm C_4C_1im}][{\rm PF_6}] < [{\rm C_4C_1im}][{\rm BF_4}] < [{\rm C_4C_1im}][{\rm SCN}].$ Based on this analysis, the ILs with the highest solubility (i.e. lowest Henry's law constants) for HFC-32 and HFC-125 are $[{\rm C_6C_1im}][{\rm FAP}]$ and $[{\rm C_4C_1im}][{\rm C_1CO_2}]$, respectively.

The ideal selectivity can also be defined as the ratio of the pure refrigerant solubilities on a molar or mass basis in the IL. The mass basis is more relevant to the design of separation systems; therefore, the selectivity can be defined as follows:

$$S_{Wij} = \left(\frac{w_{vi}/w_{li}}{w_{vj}/w_{lj}}\right)_{T,P} \tag{23}$$

where $w_{vi,j}$ and $w_{li,j}$ are the vapor and liquid mass fractions of the dissolved refrigerants (i = HFC-32 and j = HFC-125) in the IL at T = 298.15 K and P = 1.0 MPa, respectively (where w_{vi} and $w_{vj} = 1.0$).

In both cases $(S_{\rm Hij} \ and \ S_{\rm Wij})$, the IL with the highest overall selectivity for the separation of R-410A, based on the ratio of the Henry's law constants $(S_{\rm Hij})$ or the ratio of the mass fractions $(S_{\rm Wij})$ for the separation of R-410A mixture was obtained using $[C_6C_1{\rm im}][Cl]$. The ideal selectivity trends obtained with eqs 22 and 23 are shown in Figure 8.

Too often in the literature, comparisons are made of the mole fraction solubility as a function of T and P as shown in Figure 9. The most relevant comparison for designing a separation process is to evaluate the difference in the mass fraction solubility as a function of T and P as shown in Figure 10.

In some cases such as for $[C_4C_1\mathrm{im}][BF_4]$, $[C_4C_1\mathrm{im}][PF_6]$, and $[C_6C_1\mathrm{im}][FAP]$, what appears to be a large difference in the mole fraction solubility for HFC-32 and HFC-125 turns out to be only a small or negligible difference in the mass fraction solubility that is needed for designing a separation process. Alternatively, small differences in the mole fraction solubility for HFC-32 and HFC-125 in $[C_4C_1\mathrm{im}][C_1CO_2]$ and $[C_6C_1\mathrm{im}][C1]$ result in larger differences in mass fraction solubility, and therefore, these two ILs are possible candidates for the separation of R-410A.

The most suitable IL for a specific gas separation must also consider practical aspects, such as the viscosity and cost of the ILs. For example, Gómez et al., reported a dynamic viscosity of $18.1 \text{ Pa} \cdot \text{s}$ for $[C_6C_1\text{im}][Cl]$ at 298.15 K and ambient pressure that is higher than the other ILs in this study, and this must be taken into consideration in separation processes. Ideally, the ILs must also be recycled and used continuously in a separation process, such as extractive distillation. However, IL losses must be expected, whereby inexpensive ILs are more desirable for lowering the *operational expenses* (OPEX) of the separation process. Additional considerations include the toxicity and corrosivity of the IL.

3.5. Fickian Diffusion Coefficients. The diffusivity of HFCs in ILs is also required to design and develop new IL-based separation processes. The time-dependent absorption behavior of HFC-32 and HFC-125 in the ILs was analyzed using a simplified Fickian diffusion model (see Section 2.5). The calculated diffusion coefficients for HFC-32 and HFC-125 in each IL at 0.05 MPa and 298.15 K, respectively, are shown in Table 11 along with the viscosity of the ILs at 298.15 K.

The diffusion coefficient (*D*) of HFCs in the ILs is dependent on the refrigerant solubility (C_s), the viscosity of the IL, ³⁸ and the molecular radius of the solute molecule, according to the Stokes–Einstein equation. ⁵⁷ The largest *D* values for HFC-32 and HFC-125 were found in [C_6C_1 im]-[FAP] (HFC-32 $D = 19.6 \times 10^{-11}$ m² s⁻¹ and HFC-125 $D = 5.5 \times 10^{-11}$ m² s⁻¹), which has one of the lowest viscosities of the ILs tested (see the Supporting Information for details). The 3.5 times higher HFC-32 diffusion coefficient in [C_6C_1 im][FAP] can be attributed to the approximately 22% smaller molecular radius for HFC-32 (0.18 nm) relative to

HFC-125 (0.23 nm). ^{58,59} In general, the calculated diffusion coefficients are in good agreement with previous reports. ⁶⁰ For example, the diffusion coefficients for HFC-32 and HFC-125 in ILs are of the same order of magnitude, that is between 10^{-11} and 10^{-10} m²·s⁻¹, for those previously reported in other fluorinated ILs. ¹³ In addition, the diffusion coefficient for R-22 (chlorodifluoromethane, CHClF₂) in $[C_4C_1\text{im}][BF_4]$ and $[C_4C_1\text{im}][PF_6]$ reported by Minnick and Shiflett is also within the same order of magnitude $(10^{-10}$ to 10^{-11} m²·s⁻¹) as the data reported here. ²⁹ The trend in diffusion coefficient with the inverse in viscosity $(D \sim 1/\mu)$ generally holds true for HFC-32 and HFC-125, except for HFC-32 + $[C_4C_1\text{im}][C_1CO_2]$, which might indicate some chemical interaction between HFC-32 and the acetate anion $[C_1CO_2]$. Molecular modeling studies are underway to elucidate this effect.

4. CONCLUSIONS

A separation process for recycling R-410A is necessary so that HFC-32 can be reused in new HFO containing low-GWP refrigerant blends, and HFC-125 can be used as a fluorinecontaining feedstock in more sustainable products. The absorption of HFC-32 and HFC-125 in six imidazoliumbased ILs containing fluorinated and non-fluorinated anions was accurately measured using a microbalance at 298.15 K and pressures ranging from 0.05 to 1.0 MPa. HFC-32 was found to be more soluble in ILs with fluorinated anions than HFC-125, which is most likely because of hydrogen bonding between the refrigerant (CH_2F_2) and the fluorinated anion $([BF_4], [PF_6],$ and [FAP]). HFC-125 was found to be more soluble in ILs with non-fluorinated anions ($[C_1CO_2]$ and [Cl]). The [C₄C₁im][SCN] had low solubility for both HFC-32 and HFC-125 relative to the other ILs tested. These results clearly demonstrate that the anion plays a major role in governing the solubility of HFCs in ILs. In future work, molecular modeling will be used to try to elucidate the physical reason for these trends. The experimental VLE data sets were successfully correlated using the van der Waals EoS, and the model was insensitive to the choice of critical parameters (600 $< T_c <$ 1400 K and $0.5 < P_c < 5.0$ MPa). The $[C_6C_1im][Cl]$ and [C₄C₁im][C₁CO₂] ILs provided the highest ideal selectivity (2.7 to 3.5 on a mass basis) for separating R-410A at 298.15 K among the ILs studied in this work. The one-dimensional diffusion model was applied to time-dependent absorption data for each HFC/IL binary system. HFC-32 and HFC-125 had a higher diffusion coefficient in [C₆C₁im][FAP] relative to the other ILs because of its lower viscosity. HFC-32 had a higher diffusion coefficient (up to 3.5 for $[C_6C_1\text{im}][FAP]$) relative to HFC-125 because of its smaller molecular radius (0.18 nm versus 0.25 nm). Molecular simulations (Monte Carlo and molecular dynamics) are underway to better understand the unique interactions and forces between HFCs and ILs. The present work provides important insights into the solubility, diffusivity, EoS modeling, and ideal selectivity of HFC-32 and HFC-125 in ILs for the design of a separation process for recycling R-410A.

ASSOCIATED CONTENT

Supporting Information

The Supporting Information is available free of charge at https://pubs.acs.org/doi/10.1021/acs.iecr.0c02820.

Comparison of VLE data for HFC-32 in $[C_4C_1\text{im}][PF_6]$ and $[C_4C_1\text{im}][BF_4]$, and HFC-125 in $[C_4C_1\text{im}][PF_6]$;

comparison of excess Gibbs energy for HFC-32 and HFC-125 in $[C_4C_1\mathrm{im}][PF_6]$, $[C_4C_1\mathrm{im}][BF_4]$, $[C_6C_1\mathrm{im}][FAP]$, $[C_6C_1\mathrm{im}][CI]$, $[C_4C_1\mathrm{im}][C_1CO_2]$, and $[C_4C_1\mathrm{im}][SCN]$; and diffusion coefficient analysis for HFC-125 in $[C_6C_1\mathrm{im}][FAP]$ (PDF)

AUTHOR INFORMATION

Corresponding Author

Mark B. Shiflett — Department of Chemical & Petroleum Engineering and Institute for Sustainable Engineering, University of Kansas, Lawrence, Kansas 66045, United States;
orcid.org/0000-0002-8934-6192; Email: mark.b.shiflett@ku.edu

Authors

Ana Rita C. Morais – Department of Chemical & Petroleum Engineering, University of Kansas, Lawrence, Kansas 66045, United States

Abby N. Harders – Department of Chemical & Petroleum Engineering and Institute for Sustainable Engineering, University of Kansas, Lawrence, Kansas 66045, United States

Kalin R. Baca — Department of Chemical & Petroleum Engineering and Institute for Sustainable Engineering, University of Kansas, Lawrence, Kansas 66045, United States; orcid.org/0000-0002-7292-8698

Greta M. Olsen – Department of Chemical & Petroleum Engineering and Institute for Sustainable Engineering, University of Kansas, Lawrence, Kansas 66045, United States

Bridgette J. Befort — Department of Chemical & Biomolecular Engineering, University of Notre Dame, Notre Dame, Indiana 46556, United States

Alexander W. Dowling – Department of Chemical & Biomolecular Engineering, University of Notre Dame, Notre Dame, Indiana 46556, United States; orcid.org/0000-0001-9383-7499

Edward J. Maginn — Department of Chemical & Biomolecular Engineering, University of Notre Dame, Notre Dame, Indiana 46556, United States; orcid.org/0000-0002-6309-1347

Complete contact information is available at: https://pubs.acs.org/10.1021/acs.iecr.0c02820

Notes

The authors declare no competing financial interest.

ACKNOWLEDGMENTS

The authors acknowledge The Wonderful Company for their financial gift and The Chemours Company for providing the HFC-32 and HFC-125 refrigerant for this study. This material is based upon work supported by the National Science Foundation under grant no. CBET-1917480 (University of Kansas) and CBET-1917474 (University of Notre Dame), Collaborative Research: Development and Application of a Molecular and Process Design Framework for the Separation of HFC Mixtures.

REFERENCES

- (1) Bolaji, B. O. CFC refrigerants and stratospheric ozone: past, present and future. *Environmental Sustainability and Conservation in Nigeria*; Environmental Conservation and Research Team (ECRT), 2005.
- (2) United States Environmental Protection Agency. Global Greenhouse Gas Emissions Data. https://www.epa.gov/

- ghgemissions/global-greenhouse-gas-emissions-data (accessed May 17, 2020).
- (3) European Environment Agency. EEA greenhouse gas—data viewer. https://www.eea.europa.eu/data-and-maps/data/data-viewers/greenhouse-gases-viewer (accessed May 17, 2020).
- (4) Stanley, K. M.; Say, D.; Mühle, J.; Harth, C. M.; Krummel, P. B.; Young, D.; O'Doherty, S. J.; Salameh, P. K.; Simmonds, P. G.; Weiss, R. F.; et al. Increase in global emissions of HFC-23 despite near-total expected reductions. *Nat. Commun.* **2020**, *11*, 397.
- (5) Calm, J. M. The next generation of refrigerants Historical review, considerations, and outlook. *Int. J. Refrig.* **2008**, 31, 1123–1133.
- (6) European Union. Regulation (EU) No. 517/2014 of the European Parliament and of the Council of 16 April 2014 on Fluorinated Greenhouse Gases and Repealing Regulation (EC) No. 842/2006.
- (7) IPCC Fifth Assessment Report (IPCC)—Intergovernmental Panel on Climate Change, 2015.
- (8) Wang, L.; Han, X.; Li, J.; Zhan, X.; Chen, J. Hydrophobic nanosilica/polydimethylsiloxane membrane for dimethylcarbonate-methanol separation via pervaporation. *Chem. Eng. J.* **2011**, *171*, 1035–1044.
- (9) Lei, Z.; Dai, C.; Zhu, J.; Chen, B. Extractive Distillation with Ionic Liquids: A Review. AIChE J. 2014, 60, 3312–3329.
- (10) Belafi-Bakó, K.; Nemestóthy, N.; Bakonyi, P. Separation of gases using membranes containing ionic liquids. In *Ionic Liquids in Separation Technology*, Elsevier: 2014; pp 261–273.
- (11) Iarikov, D. D.; Hacarlioglu, P.; Oyama, S. T. Supported room temperature ionic liquid membranes for CO₂/CH₄ separation. *Chem. Eng. J.* **2011**, *166*, 401–406.
- (12) Mahurin, S. M.; Lee, J. S.; Baker, G. A.; Luo, H.; Dai, S. Performance of nitrile-containing anions in task-specific ionic liquids for improved CO₂/N₂ separation. *J. Membr. Sci.* **2010**, 353, 177–183.
- (13) Shiflett, M. B.; Yokozeki, A. Solubility and diffusivity of hydrofluorocarbons in room-temperature ionic liquids. *AIChE J.* **2006**, 52, 1205–1219.
- (14) Shiflett, M. B.; Yokozeki, A. Separation of difluoromethane and pentafluoroethane by extractive distillation using ionic liquid. *Chim. Oggi.* **2006**, *24*, 28–30.
- (15) Sosa, J. E.; Ribeiro, R. P. P. L.; Castro, P. J.; Mota, J. P. B.; Araújo, J. M. M.; Pereiro, A. B. Absorption of Fluorinated Greenhouse Gases Using Fluorinated Ionic Liquids. *Ind. Eng. Chem. Res.* **2019**, *58*, 20769–20778.
- (16) Liu, X.; Pan, P.; He, M. Vapor-liquid equilibrium and diffusion coefficients of R32+[HMIM][FEP], R152a+[HMIM][FEP] and R161+[HMIM][FEP]. *J. Mol. Liq.* **2018**, 253, 28–35.
- (17) Liu, X.; Lv, N.; Su, C.; He, M. Solubilities of R32, R24Sfa, R227ea and R236fa in a phosphonium-based ionic liquid. *J. Mol. Liq.* **2016**, 218, 525–530.
- (18) Liu, X.; He, M.; Lv, N.; Qi, X.; Su, C. Vapor-liquid equilibrium of three hydrofluorocarbons with [HMIM][Tf₂N]. *J. Chem. Eng. Data* **2015**, *60*, 1354–1361.
- (19) Sousa, J. M. M. V.; Granjo, J. F. O.; Queimada, A. J.; Ferreira, A. G. M.; Oliveira, N. M. C.; Fonseca, I. M. A. Solubilities of hydrofluorocarbons in ionic liquids: Experimental and modelling study. *J. Chem. Thermodyn.* **2014**, *73*, 36–43.
- (20) Asensio-Delgado, S.; Pardo, F.; Zarca, G.; Urtiaga, A. Vapor–Liquid Equilibria and Diffusion Coefficients of Difluoromethane, 1, 1, 1, 2-Tetrafluoroethane, and 2, 3, 3, 3—Tetrafluoropropene in Low-Viscosity Ionic Liquids. *J. Chem. Eng. Data* **2020**, 65, 4242.
- (21) Lemmon, E. W.; Huber, M. L.; McLinden, M. O. NIST Reference Fluid Thermodynamic and Transport Properties—REFPROP 10.0: Gaithersburg, Maryland, 2013.
- (22) Shiflett, M. B.; Harmer, M. A.; Junk, C. P.; Yokozeki, A. Solubility and diffusivity of 1,1,1,2-tetrafluoroethane in room-temperature ionic liquids. *Fluid Phase Equilib.* **2006**, 242, 220–232.
- (23) Freire, M. G.; Neves, C. M. S. S.; Marrucho, I. M.; Coutinho, J. A. P.; Fernandes, A. M. Hydrolysis of Tetrafluoroborate and Hexafluorophosphate Counter Ions in Imidazolium-Based Ionic Liquids. *J. Phys. Chem. A* **2010**, *114*, 3744–3749.

- (24) Minnick, D. L.; Turnaoglu, T.; Rocha, M. A.; Shiflett, M. B. Review Article: Gas and vapor sorption measurements using electronic beam balances. *J. Vac. Sci. Technol., A* **2018**, *36*, 050801.
- (25) Shiflett, M. B.; Yokozeki, A. Solubilities and diffusivities of carbon dioxide in ionic liquids: $[pF_6]$ and $[pF_6]$ and $[pF_4]$. Ind. Eng. Chem. Res. 2005, 44, 4453–4464.
- (26) Yokozeki, A.; Shiflett, M. B. Global phase behaviors of trifluoromethane in ionic liquid [bmim][PF6]. *AIChE J.* **2006**, *52*, 3952–3957.
- (27) Yokozeki, A.; Shiflett, M. B. Vapor-liquid equilibria of ammonia+ ionic liquid mixtures. *Appl. Energy* **2007**, *84*, 1258–1273.
- (28) Shiflett, M. B.; Yokozeki, A. Solubility and diffusivity of hydrofluorocarbons in room-temperature ionic liquids. *AIChE J.* **2006**, *52*, 1205–1219.
- (29) Minnick, D. L.; Shiflett, M. B. Solubility and Diffusivity of Chlorodifluoromethane in Imidazolium Ionic Liquids: $[emim][Tf_2N]$, $[bmim][BF_4]$, $[bmim][PF_6]$, and [emim][TFES]. Ind. Eng. Chem. Res. **2019**, 58, 11072–11081.
- (30) Shojaeian, A.; Fatoorehchi, H. Modeling solubility of refrigerants in ionic liquids using Peng Robinson-Two State equation of state. *Fluid Phase Equilib.* **2019**, *486*, 80–90.
- (31) Sousa, J. M. M. V.; Granjo, J. F. O.; Queimada, A. J.; Ferreira, A. G. M.; Oliveira, N. M. C.; Fonseca, I. M. A. Solubility of hydrofluorocarbons in phosphonium-based ionic liquids: Experimental and modelling study. *J. Chem. Thermodyn.* **2014**, *79*, 184–191.
- (32) Orbey, H.; Sandler, S. I. Equation of state modeling of refrigerant mixtures. *Ind. Eng. Chem. Res.* **1995**, *34*, 2520–2525.
- (33) Teodorescu, M.; Lugo, L.; Fernandez, J. Modeling of gas solubility data for HFCs-lubricant oil binary systems by means of the SRK equation of state. *Int. J. Thermophys.* **2003**, *24*, 1043–1060.
- (34) Fernández, W.; Sensenich, B.; Scurto, A. M. High-pressure phase equilibria of {carbon dioxide (CO₂) + n-alkyl-imidazolium bis(trifluoromethylsulfonyl) amide} ionic liquids. *J. Chem. Thermodyn.* **2010**, *42*, 305–311.
- (35) Yokozeki, A.; Shiflett, M. B. Gas solubilities in ionic liquids using a generic van der Waals equation of state. *J. Supercrit. Fluids* **2010**, *55*, 846–851.
- (36) Yokozeki, A. Solubility of refrigerants in various lubricants. *Int. J. Thermophys.* **2001**, *22*, 1057–1071.
- (37) Shiflett, M. B.; Yokozeki, A. Gaseous absorption of fluoromethane, fluoroethane, and 1,1,2,2-tetrafluoroethane in 1-butyl-3-methylimidazolium hexafluorophosphate. *Ind. Eng. Chem. Res.* **2006**, 45, 6375–6382.
- (38) Yokozeki, A. Time-dependent behavior of gas absorption in lubricant oil. *Int. J. Refrig.* **2002**, *25*, 695–704.
- (39) Ren, W.; Scurto, A. M. Phase equilibria of imidazolium ionic liquids and the refrigerant gas, 1,1,1,2-tetrafluoroethane (R-134a). *Fluid Phase Equilib.* **2009**, 286, 1–7.
- (40) Shiflett, M. B.; Harmer, M. A.; Junk, C. P.; Yokozeki, A. Solubility and diffusivity of difluoromethane in room-temperature ionic liquids. *J. Chem. Eng. Data* **2006**, *51*, 483–495.
- (41) Egorova, K. S.; Ananikov, V. P. Toxicity of ionic liquids: eco (cyto) activity as complicated, but unavoidable parameter for task-specific optimization. *Chemsuschem* **2014**, *7*, 336–360.
- (42) Street, K. W., Jr; Morales, W.; Koch, V. R.; Valco, D. J.; Richard, R. M.; Hanks, N. Evaluation of vapor pressure and ultra-high vacuum tribological properties of ionic liquids. *Tribol. Trans.* **2011**, *54*, 911–919.
- (43) Rebelo, L. P. N.; Canongia Lopes, J. N.; Esperança, J. M. S. S.; Filipe, E. On the Critical Temperature, Normal Boiling Point, and Vapor Pressure of Ionic Liquids. *J. Phys. Chem. B* **2005**, *109*, 6040–6043.
- (44) Rai, N.; Maginn, E. J. Critical behaviour and vapour-liquid coexistence of 1-alkyl-3-methylimidazolium bis (trifluoromethylsulfonyl) amide ionic liquids via Monte Carlo simulations. *Faraday Discuss.* **2012**, *154*, 53–69.
- (45) Valderrama, J. O.; Rojas, R. E. Critical properties of ionic liquids. *Ind. Eng. Chem. Res.* **2009**, 48, 6890–6900.
- (46) Bard, Y. Nonlinear Parameter Estimation; Academic Press, 1974.

- (47) Bevington, P.; Robinson, D. Data Reduction and Error Analysis for the Physical Sciences, 3rd ed.; McGraw-Hill: New York City, 2003; pp 194–218.
- (48) Chis, O.-T.; Villaverde, A. F.; Banga, J. R.; Balsa-Canto, E. On the relationship between sloppiness and identifiability. *Math. Biosci.* **2016**, 282, 147–161.
- (49) Moura, L.; Mishra, M.; Bernales, V.; Fuentealba, P.; Padua, A. A. H.; Santini, C. C.; Costa Gomes, M. F. Effect of unsaturation on the absorption of ethane and ethylene in imidazolium-based ionic liquids. *J. Phys.Chem. B.* **2013**, *117*, 7416–7425.
- (50) Gómez, E.; González, B.; Domínguez, Á.; Tojo, E.; Tojo, J. Dynamic viscosities of a series of 1-alkyl-3-methylimidazolium chloride ionic liquids and their binary mixtures with water at several temperatures. *J. Chem. Eng. Data* **2006**, *51*, 696–701.
- (51) Moganty, S. S.; Baltus, R. E. Diffusivity of carbon dioxide in room-temperature ionic liquids. *Ind. Eng. Chem. Res.* **2010**, 49, 9370–9376
- (52) Safarov, J.; Geppert-Rybczyńska, M.; Kul, I.; Hassel, E. Thermophysical properties of 1-butyl-3-methylimidazolium acetate over a wide range of temperatures and pressures. *Fluid Phase Equilib.* **2014**, 383, 144–155.
- (53) Ahosseini, A.; Scurto, A. M. Viscosity of imidazolium-based ionic liquids at elevated pressures: Cation and anion effects. *Int. J. Thermophys.* **2008**, *29*, 1222–1243.
- (54) Gao, J.; Wagner, N. J. Non-ideal viscosity and excess molar volume of mixtures of 1-butyl-3-methylimidazolium tetrafluoroborate ($[C_4mim][BF_4]$) with water. J. Mol. Liq. 2016, 223, 678–686.
- (55) Li, J.-G.; Hu, Y.-F.; Ling, S.; Zhang, J.-Z. Physicochemical properties of $[C_6 mim][PF_6]$ and $[C_6 mim][(C_2F_5)_3PF_3]$ ionic liquids. *J. Chem. Eng. Data* **2011**, *56*, 3068–3072.
- (56) Domańska, U.; Królikowska, M. Density and viscosity of binary mixtures of {1-butyl-3-methylimidazolium thiocyanate+ 1-heptanol, 1-octanol, 1-nonanol, or 1-decanol}. *J. Chem. Eng. Data* **2010**, *55*, 2994–3004.
- (57) Reid, R. C.; Prausnitz, J. M.; Poling, B. E. The Properties of Gases and Liquids; McGraw Hill: New York, USA, 1987.
- (58) Yokozeki, A.; Sato, H.; Watanabe, K. Ideal-gas heat capacities and virial coefficients of HFC refrigerants. *Int. J. Thermophys.* **1998**, 19, 89–127.
- (59) Morais, A. R. C.; Simoni, L. D.; Douglas, J. T.; Scurto, A. M.; Shiflett, M. B. Phase Equilibrium and Diffusivities of Hydrofluorocarbons in a Synthetic Polyol Ester Lubricant. *AIChE J.* **2020**, *66*, No. e16241.
- (60) Gessner, T. R.; Barbosa, J. R., Jr Modeling absorption of pure refrigerants and refrigerant mixtures in lubricant oil. *Int. J. Refrig.* **2006**, 29, 773–780.